RSC Advances

PAPER

View Article Online
View Journal | View Issue

Cite this: *RSC Adv.*, 2024, **14**, 34228

Ionic resorcinarenes as drug solubilization agents in water†

Frank Boateng Osei, [a] Kwaku Twum, [a] Barbara Manfredi, [b] Mariana Fatohi, [a] Yvonne Bessem Ojong, [a] Valance Washington[b] and Ngong Kodiah Beyeh *[a]

Received 16th September 2024
Accepted 15th October 2024

DOI: 10.1039/d4ra06682k

rsc.li/rsc-advances

Resorcinarenes are capable of host–guest complexation with small molecules, however, they are less studied as pharmaceutical drug delivery aids. This article reports on the aqueous-solubility enhancing effect of an octa-sulfonated resorcinarene and a C-hydroxybenzyl ammonium resorcinarene chloride on three hydrophobic drugs: isoniazid, caffeine, and griseofulvin. The findings are backed by dynamic light scattering, isothermal calorimetric titration, and nuclear magnetic resonance experiments in water. Aqueous mixtures of equal volumes of drug compounds and resorcinarene solutions produced a more soluble and clearer unit than solutions of pure drug compounds in water. Light scattering experiments revealed shifts in particle sizes of pure drug compounds to the range of resorcinarene hosts. ^{1}H NMR measurements of resorcinarene-drug mixtures confirmed interactions with shift changes ranging from −0.20 to 0.81 ppm. Binding affinities quantified through ITC experiments ranged between 0.54 and 211 mM, signifying interactions between resorcinarenes and drug compounds necessary for the solubility of the drugs. Cytotoxicity studies suggest that resorcinarenes alone, or complexed with any of the drug compounds, do not exert cytotoxicity in mammalian cells HEK-293 up to 200 μM. We herein propose a set of hydrophilic resorcinarene macrocycles as potential drug solubilizers.

Introduction

Resorcinarenes are widely investigated organic macrocycles for their host properties towards many guest systems.[1–3] They interact with other molecular guests through multiple non-covalent interactions within their well-defined internal cavities.[4–7] These host–guest interactions confer various properties on the guest molecules, which include solubility modifications, guest-release modifications, enhanced targeting, enhanced stability, and milder side effects in the case of drug agents.[8–12] Drug solubility in aqueous environments, including that of the human body, is a major challenge in the pharmaceutical industry.[13,14] The biopharmaceutical classification system (BCS) defines groups II and IV drugs as having lower solubility, which inhibits their gastrointestinal absorption, permeability, and efficacy.[15,16] Enhancing the solubility of hydrophobic drugs plays a key role in formulation development as it enhances the bioavailability and therapeutic action of drugs at their target sites.[17–19] Methods for enhancing drug solubility include particle size reduction through micronization[20] and nanosuspension,[21] modification of the crystal nature of the active pharmaceutical ingredient through crystal engineering, polymorphism, and use of hydrated or solvated forms of the drugs,[22] drug dispersion in carriers,[23] complexation techniques, and chemical modifications.[24]

Griseofulvin is an antifungal agent mainly used to treat Tinea capitis infections, especially in children.[25] It belongs to BCS group II drugs[26] and is known to have low aqueous solubility, leading to low bioavailability.[27] Methods that have been studied in the solubility enhancement of griseofulvin include nanoformulation techniques and melt granulation.[28,29] Other BCS groups I and III drugs are known to have varying degrees of solubility that affect their permeability and bioavailability. Isoniazid, an anti-tubercular agent, is reported to be on the borderline of groups I and III because lactose and other deoxidizing saccharides can form condensation products with isoniazid, which limits its permeability.[30] This calls for solid dosage forms of isoniazid that are very rapidly dissolving.[30] Methods, such as cocrystal formation, have been employed to enhance the aqueous solubility and subsequent drug release.[31] Caffeine, a psychomotor stimulant, is known to be hydrophobic in nature due to a planar purine structure and the presence of 3-methyl groups and, therefore, weakly polar in water undergoing oligomerization and aggregation in aqueous solutions, which limits its bioavailability and efficacy.[32,33] Methods such as the use of sugars and deep eutectic solvents have been employed in enhancing the aqueous solubility of caffeine.[33,34]

[a]*Oakland University, Department of Chemistry, 146 Library Drive, Rochester, MI 48309-4479, USA. E-mail: beyeh@oakland.edu*

[b]*Oakland University, Department of Biological Sciences, 146 Library Drive, Rochester, MI 48309-4479, USA*

† Electronic supplementary information (ESI) available: Experimental details, copies of ^{1}H NMR, ITC, and DLS data. See DOI: https://doi.org/10.1039/d4ra06682k

Water-soluble resorcinarenes are not cytotoxic, especially at lower concentrations, and have been shown to exhibit proper biodegradability and biocompatibility, making them attractive in improving drug solubility.[35] In this work, we explore the interactions between two synthetic ionic water-soluble resorcinarene macrocycles (**R1** and **R2**, (Fig. 1)) and three hydrophobic drugs, isoniazid, caffeine, and griseofulvin (**ISO**, **CAF**, and **GRI**, (Fig. 1)). Herein, we investigate two water-soluble resorcinarenes that successfully interact and solubilize three drugs through a combination of NMR, isothermal titration calorimetry, and cytotoxicity analyses.

Materials and methods

Synthesis of resorcinarene receptors and guests

In this study, we selected two water-soluble resorcinarenes receptors. The first receptor is an octa-anionic poly-sulfonated resorcinarene with both the upper and lower rims decorated with sulfonate groups. A two-phase mixture of 2-(2-bromoethyl)-1,3-dioxane, **1** (20 mmol) and an aqueous solution (20 mL) of Na_2SO_3, **2** (40 mmol) was stirred at 100 °C for 24 hours. Water (20 mL) was added to the resulting homogeneous solution, and the mixture was washed with ether (40 mL × 2) to eliminate unreacted **1**. To this mixture was added ethanol (40 mL), resorcinol, **3** (36 mmol), and concentrated HCl (6 mL). The mixture was stirred under nitrogen at 100 °C on a VWR® hotplate/stirrer for 24 h. After reflux, the solvent was evaporated, and the residue was taken in water (60 mL) and dialyzed three times against water (2 L) using a dialysis membrane with a transport critical molecular weight of 1000 (Spectra/Por membrane MWCO 1000) to remove inorganic salts. Most of the water was removed under vacuum, and the residue was triturated from cold methanol to give the lower rim sulfonated resorcinarene, **4** (Fig. 2). Resorcinarene **4** (0.01 mol), a solution

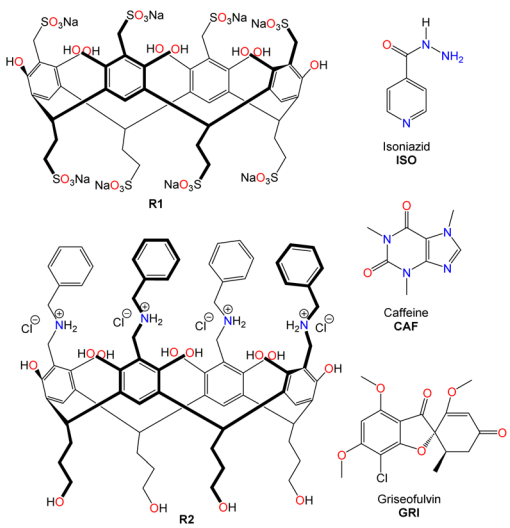

Fig. 1 Structures of octa-sulfonated resorcinarene (R1) and C-hydroxybenzylammonium resorcinarene chloride (R2) as hosts, and drug compounds: isoniazid (ISO), caffeine (CAF) and griseofulvin (GRI) as guests.

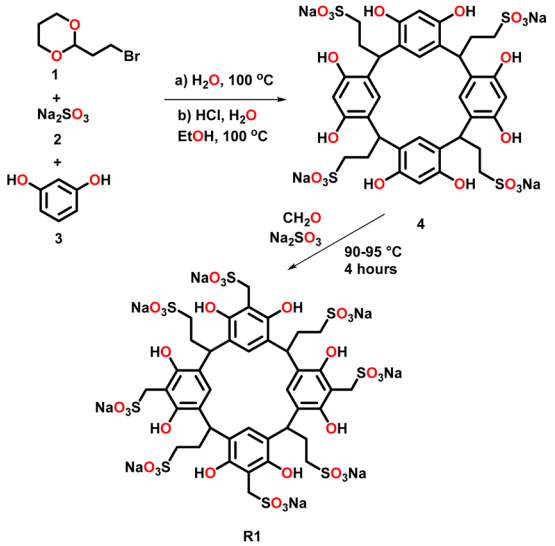

Fig. 2 Schematic representation of the synthesis of R1 with 4 as an intermediate.

of 37% formaldehyde (0.01 mol) and sodium sulfite (0.01 M) in H_2O (30 mL) was stirred and heated at 90–95 °C for 4 h. Dilute hydrochloric acid was added after cooling until pH 7, then methanol (50 mL or more) was added to precipitate the product **R1**. The solid was filtered and dried (Fig. 2 and S1–S4†).

The second receptor is a tetra-cationic resorcinarene with the cationic groups on the upper rim and four hydroxyl groups on the lower rim for enhanced solubility. This cationic receptor also possesses four flexible benzyl units with the potential to interact with the aromatic fragments of the drugs. The synthesis of this macrocycle is reported elsewhere (Fig. S5 and S6†).[36–38] Both resorcinarene macrocycles exist in the C_{4v} conformation with a persistent hydrophobic cavity. For this pilot study, three drugs, isoniazid, **ISO**, caffeine, **CAF**, and griseofulvin, **GRI**, were selected. These drugs were selected due to their hydrophobic nature and very limited solubility in water. In addition, they all possess pyridinium, imidazolium, and methyl phenolic aromatic groups, respectively, which can interact with different components of the two resorcinarenes receptors. All the drugs were purchased from Sigma Aldrich.

Dynamic light scattering (DLS) experiments

Dynamic light scattering measurements were performed to determine the particle size distributions within associations between host and guest molecules, which can be a determinant of the solubility of drugs. This technique has been employed to study the solubility of drugs such as doxorubicin, hydrochlorothiazide, lamotrigine, erythromycin, ibuprofen, and aspirin.[39–42] DLS was conducted using a Malvern® zetasizer Nano from Malvern Panalytical to measure the particle size distribution of drug compounds alone and in combination with macrocycles. The Malvern Instruments DLS device (Zetasizer Nano ZS Series) has a 4 mW He–Ne ion laser at a wavelength of 633 nm and an avalanche photodiode detector at an angle of 173°. Experiments were carried out at 25 °C. Plastibrand semi-

Table 1 Thermodynamic binding parameters of formed complexes between the host and the guests by ITC[a]

	$K_a \times 10^3$ (M^{-1})	ΔH (kcal mol^{-1})	$T\Delta S$ (kcal mol^{-1})	ΔG (kcal mol^{-1})
CAF@R1	$K_1 = 5.36 \pm 0.30$	-0.86 ± 0.77	4.23	-5.10 ± 0.77
	$K_2 = 0.54 \pm 0.16$	2.24 ± 0.81	5.96	-3.72 ± 0.81
CAF@R2	$K_1 = 58.40 \pm 5.48$	-0.11 ± 0.01	6.41	-6.51 ± 0.01
	$K_2 = 1.97 \pm 0.15$	1.21 ± 0.04	5.69	-4.48 ± 0.04
GRI@R1	$K_1 = 10.94 \pm 6.01$	0.18 ± 0.23	5.69	-5.51 ± 0.20
	$K_2 = 0.68 \pm 0.25$	2.69 ± 0.83	6.56	-3.86 ± 0.83
[b] **GRI@R2**	$K = 24.50 \pm 2.60$	3.54 ± 0.10	9.51	-5.97 ± 0.10
ISO@R1	$K_1 = 211.25 \pm 60.01$	-0.66 ± 0.03	6.58	-7.25 ± 0.03
	$K_2 = 1.99 \pm 0.16$	0.31 ± 0.01	4.83	-4.51 ± 0.01
[b] **ISO@R2**	$K = 2.14 \pm 0.90$	1.72 ± 1.47	6.26	-4.53 ± 1.47

[a] ITC was done in H_2O at 298 K and fitted to two binding sites. [b] Fit to one binding site.

micro PMMA cuvettes were used to measure the size. Zetasizer software (Malvern Instruments) was used to obtain the particle size distributions. Equimolar concentration samples were prepared in deionized water. DLS experiments involved 1 mL of each pure sample. Mixtures were prepared by pipetting 1 mL of drug compound solution and 1 mL of resorcinarene into a clean cuvette.

Nuclear magnetic resonance (NMR)

NMR is a suitable method to study the interaction between organic species in solution by monitoring changes between the isolated components and the physical mixtures. This technique also provides information on the orientation of the drug in the macrocycle. ^{1}H and ^{13}C NMR are useful as the chemical and electronic environments of the protons and/or carbons are affected in macrocycle-drug complexations.[42] This method has been used to assess the solubility of drugs such as ibuprofen and carbamazepine.[43–45] The qualitative binding properties of drugs as guests towards hosts **R1-2** were probed in solution through ^{1}H NMR experiments. The interaction between the host and guest in deuterated water was observed from equimolar mixtures of both species. Spectra were recorded on a Bruker Avance DRX 400 spectrometer (400 MHz for ^{1}H). All signals are given as δ values in ppm using residual solvent signals as the internal standard. For sample preparation, stock solutions of the macrocycles **R1-2** (5 mg mL^{-1}) and drug compounds (10 mg mL^{-1}) were prepared in D_2O. For pure sample measurements, 250 μL of the 5 mg mL^{-1} stock solution was measured in NMR tube and diluted with 250 μL of D_2O. To measure possible binding interactions for a 1 : 1 host–guest complex, 250 μL of

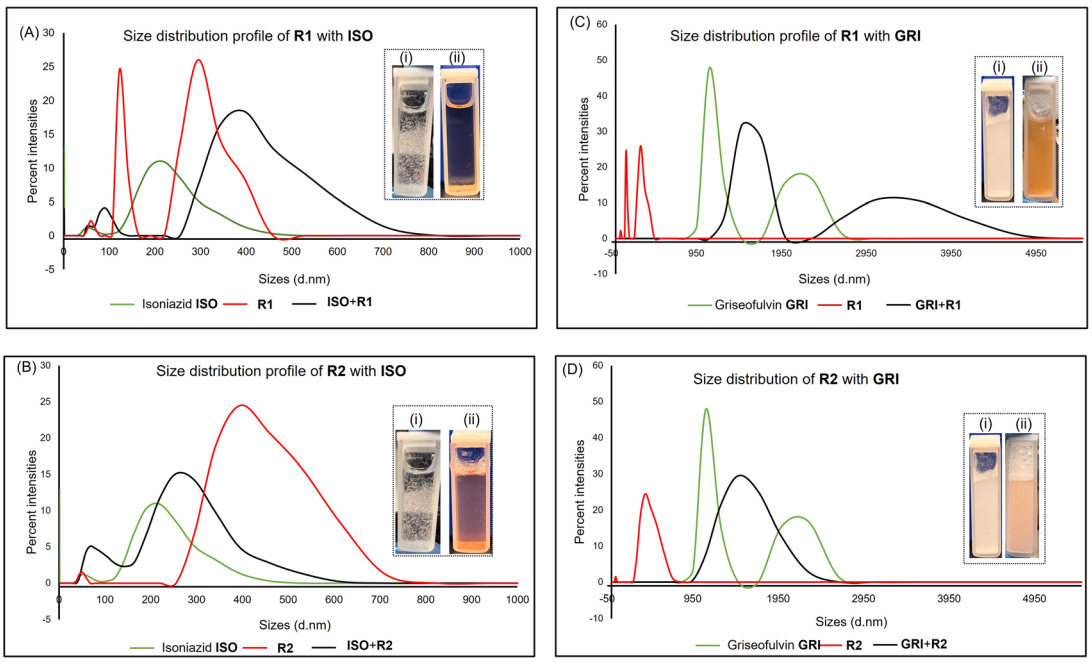

Fig. 3 Illustration of the dynamic light scattering (DLS) experiment showing the size distribution profile of the pure drug, pure receptor, and equimolar mixtures of the receptor and the drugs (A) **R1** + **ISO**, (B) **R1** + **GRI**, (C) **R2** + **ISO**, (D) **R2** + **GRI**. Inset: picture showing (i) the pure drug and (ii) the equimolar receptor-drug mixtures, respectively.

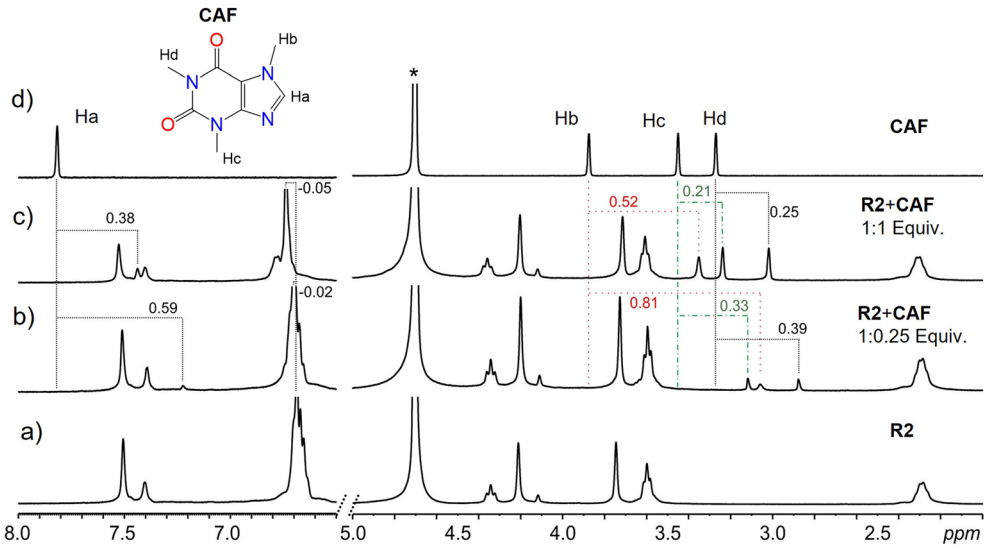

Fig. 4 Sections of the ^{1}H NMR spectra in D_2O at 298 K of pure (a) receptor **R2** and (d) drug **CAF**, and mixtures of **R2** and **CAF** (b) 1 : 0.25 eq and (c) 1 : 1 eq. The broken lines and colors indicate the signal changes in ppm. The star represents the residual D_2O solvent.

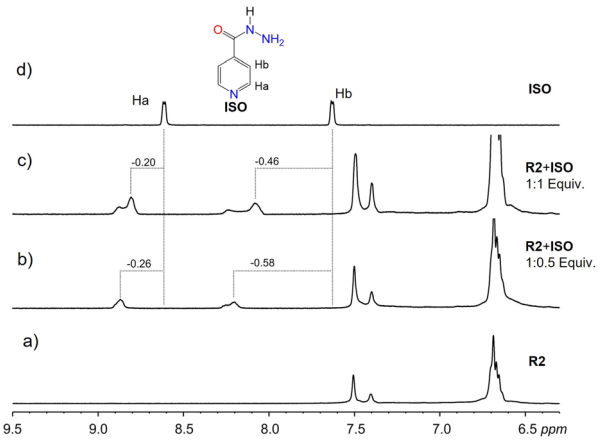

Fig. 5 Sections of the ^{1}H NMR spectra in D_2O at 298 K of pure (a) receptor **R2** and (d) drug **ISO**, and mixtures of **R2** and **ISO** (b) 1 : 0.5 eq and (c) 1 : 1 eq. The dashed lines indicate the signal changes in ppm.

5 mg mL^{-1} of a sample drug and 250 μL of 5 mg mL^{-1} of a host were measured into an NMR sample tube to give a resulting mixture of 2.5 mg mL^{-1} of both samples. Due to the very low aqueous solubility of **GRI**, NMR measurements in deuterated water were not possible.

Isothermal calorimetric (ITC) titrations

ITC titrations are useful in obtaining the quantitative parameters related to interactions between the drug compounds and macrocyclic hosts **R1-2**. This approach has been used in studying the effects of cyclodextrin and surfactants on the solubility of drug compounds such as simvastatin and sertaconazole.[42,46,47] The complexation of the drug guests by the host **R1-2** was quantified through a series of ITC experiments in deionized water. This was carried out by filling the sample cell with a receptor and the drug sample as titrants in the syringe in a 1 : 10 molar ratios. Titrations were done *via* a computer-automated injector at 298 K. The thermodynamic parameters of host–guest binding (K_a, ΔH, ΔS, and ΔG) were determined by fitting the ITC data to one and two-site binding models (Table 1).

Cell culture

HEK-293 cells (ATCC CRL-11268) were maintained in complete media as a datasheet. All cultures were incubated at 37 °C and 5% CO_2. All cells were tested for mycoplasma (data not shown) as a kit datasheet (rep-mys-10 by InvivoGen, San Diego, CA). Cells had at least 95% viability by Trypan Blue Exclusion Assay (15250-061, Gibco, Billings, MT), and not exceeded passage 30 (data not shown).

MTT assay

HEK-293 were seeded in cell-culture-treated 96 multiwell plates (CytoOne CC7682-7596, USA Scientific Inc., Ocala, FL, USA), in complete media at a concentration of 40 000 cells per well resuspended in 100 μL per well and incubated at 37 °C overnight. The media was replaced with complete media containing the compounds of interest at increasing concentration up to 2000 μM. Plates were incubated at 37 °C up to 20 or 68 hours, after which cells were assayed with 10 μL of 5 mg mL^{-1} MTT reagent (Calbiochem, San Diego, CA, USA) in ultra-purified water for 4 hours. Formazan crystals were dissolved in the incubator overnight with 100 μL of a stop solution (80% 2-propanol, 10% 1 N HCl, and 10% Triton X-100). A Tecan plate-reader model Spark (Tecan Austria GmbH, Grödig, Austria) and Magellan software or Epoch microplate (BioTek Instruments, Winooski, VT, USA) and Microsoft Excel software were used to detect colorimetric changes measured at A570 (test) and A690 (reference) wavelengths. Absorbance was normalized to untreated controls using Microsoft Excel software. Statistical

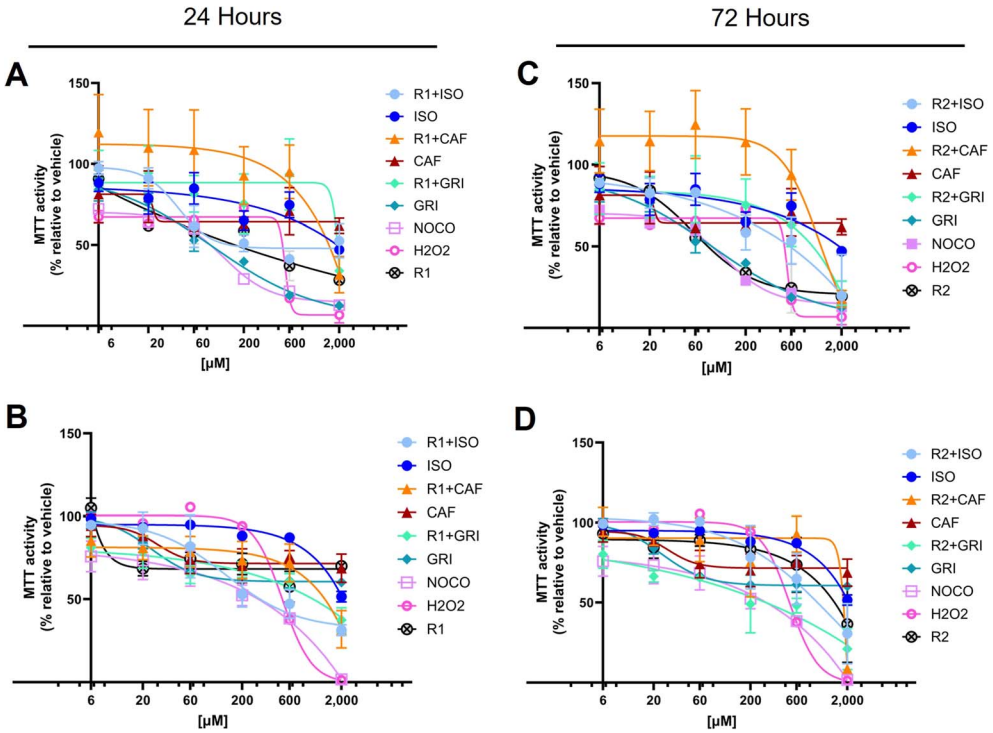

Fig. 6 Compounds assayed for inferred cytotoxicity (MTT assay). HEK-293 cells were incubated with a combination of carriers **R1** or **R2** and caffeine (**CAF**) or griseofulvin (**GRI**) or isoniazid (**ISO**) to infer cytotoxicity *via* MTT assay. Compounds are assayed at increasing concentrations up to 2000 μM for 24 (A and B) or 72 (C and D) hours. Percentage of MTT activity, shows inferred cytotoxicity relative to the vehicle DMSO that serves as negative control. Nocodazole or H_2O_2 serve as positive control. Data are representative of at least three biological replicates (mean ± SD), in technical triplicates. Two-way ANOVA Tukey's multiple comparison test.

analyses (significance set at $p < 0.05$) were performed using GraphPad Prism version 10.0. Assays were performed at least as two independent experiments, repeated in at least three biological replicates, and in technical replicates, when possible, unless otherwise stated. Data were presented as mean values ± standard deviation (SD).

Crystal violet assay

Cells were seeded in 6 multiwell plates (CC7682-7506, CytoOne, USA) at a concentration of 0.5×10^6 per well in a final volume of 2 mL per well and let adhere overnight. Cells were treated for 24 or 72 hours with a low (6 μM) or high (200 μM) concentration of compounds of interest or controls. DMSO vehicle serves as negative control, and nocodazole (in DMSO) 500 μM or hydrogen peroxide (H_2O_2) 200 μM serve as positive controls. Bright field microscope (Nikon) pictures of the cells were taken after fixing them with paraformaldehyde (PFA) 4% 20 minutes at room temperature and gently washing the wells to remove unattached cells. Cells were stained with 0.05% (w/v) crystal violet solution for 10 minutes (Sigma-Aldrich, Milwaukee, WI, USA) and distained with 10% acetic acid solution using a benchtop shaker for 30 minutes (Thermo Fisher Scientific, Waltham, MA, USA). A plate reader model Epoch (BioTek Instruments, Winooski, VT, USA) was used to measure the absorbance at 570 nm in three biological replicates in technical triplicate. Relative viability (%), calculated from the raw data of background signal subtracted from the optical density (OD), was plotted in GraphPad Prism software.

Results and discussion

Synthesis of receptor **R1** starts with resorcinarene **4**, which was synthesized using established procedures.[48] Resorcinarene **4**, in the presence of sodium sulfite and 37% formaldehyde, undergoes electrophilic aromatic substitution, leading to sulfonation of the upper rim (Fig. 2). Full characterization through HRMS, ^{1}H, and ^{13}C NMR confirmed the purity of the compound (Fig. S2 and S4†).

Light scattering experiments revealed that in isolation, molecules of the drugs **ISO**, **CAF**, and **GRI** formed smaller-sized assemblies as compared to the hydrophilic host **R1** and **R2**. A mixture of **ISO** and **R1** led to larger assemblies, which can be attributed to the complexation of **ISO** to **R1**, enhancing the former's solubility in water. This association can be evident in the differences in the clarity of solutions of **ISO** in water and **ISO-R1** mixture in water (Fig. 3). A similar observation was made in the molecular size distribution of **GRI** and **GRI-R1** mixture. However, the effect of host **R1** on the solubility of **ISO** is greater than that of **GRI** (Fig. 3). This may be attributed to stronger host–guest interaction between **ISO** and **R1** due to enhanced complementarity of weak interactions. Molecules of **ISO** and **GRI** formed respective assemblies with host **R2**, the sizes of which are skewed towards the sizes of the molecules of the host

Table 2 Statistical analysis for the main compounds assayed in Fig. 6 for inferred cytotoxicity (MTT assay). Compounds are assayed alone or in combination with **R1** at increasing concentrations up to 2000 μM for 24 (left) or 72 (right) hours. Data are representative of at least three biological replicates (mean ± SD), in technical triplicates. Two-way ANOVA Tukey's multiple comparison test

Tukey's multiple comparison test (24 h, **R1**)	Summary	Adjusted *P* value	Tukey's multiple comparison test (72 h, **R1**)	Summary	Adjusted *P* value
6 μM			6 μM		
R1 + **ISO** *vs.* **ISO**	ns	0.9733	**R1** + **ISO** *vs.* **ISO**	ns	0.9989
R1 + **CAF** *vs.* **CAF**	***	0.0004	**R1** + **CAF** *vs.* **CAF**	ns	0.7833
R1 + **GRI** *vs.* **GRI**	ns	0.8149	**R1** + **GRI** *vs.* **GRI**	ns	0.0834
20 μM			20 μM		
R1 + **ISO** *vs.* **ISO**	ns	0.8647	**R1** + **ISO** *vs.* **ISO**	ns	>0.9999
R1 + **CAF** *vs.* **CAF**	*	0.0127	**R1** + **CAF** *vs.* **CAF**	ns	0.9297
R1 + **GRI** *vs.* **GRI**	ns	0.4547	**R1** + **GRI** *vs.* **GRI**	ns	0.9821
60 μM			60 μM		
R1 + **ISO** *vs.* **ISO**	ns	0.1249	**R1** + **ISO** *vs.* **ISO**	ns	0.3059
R1 + **CAF** *vs.* **CAF**	****	<0.0001	**R1** + **CAF** *vs.* **CAF**	ns	0.9954
R1 + **GRI** *vs.* **GRI**	*	0.0247	**R1** + **GRI** *vs.* **GRI**	ns	>0.9999
200 μM			200 μM		
R1 + **ISO** *vs.* **ISO**	ns	0.7657	**R1** + **ISO** *vs.* **ISO**	****	<0.0001
R1 + **CAF** *vs.* **CAF**	*	0.0158	**R1** + **CAF** *vs.* **CAF**	ns	0.9994
R1 + **GRI** *vs.* **GRI**	**	0.0013	**R1** + **GRI** *vs.* **GRI**	ns	0.9526
600 μM			600 μM		
R1 + **ISO** *vs.* **ISO**	**	0.0037	**R1** + **ISO** *vs.* **ISO**	****	<0.0001
R1 + **CAF** *vs.* **CAF**	ns	0.0992	**R1** + **CAF** *vs.* **CAF**	ns	0.9987
R1 + **GRI** *vs.* **GRI**	****	<0.0001	**R1** + **GRI** *vs.* **GRI**	ns	>0.9999
2000 μM			2000 μM		
R1 + **ISO** *vs.* **ISO**	ns	0.9992	**R1** + **ISO** *vs.* **ISO**	*	0.0111
R1 + **CAF** *vs.* **CAF**	*	0.0132	**R1** + **CAF** *vs.* **CAF**	****	<0.0001
R1 + **GRI** *vs.* **GRI**	ns	0.2073	**R1** + **GRI** *vs.* **GRI**	**	0.0022

R2, indicative of host–guest interactions between **ISO**, **GRI**, and **R2**. A similar trend in particle size distribution has been reported by Patel *et al.*[49] by using an amphiphilic cyclodextrin to enhance the solubility and release of the hydrophobic drug tamoxifen citrate. The association of **ISO** to **R2** produced a clearer solution than **GRI**, which may be due to better complementarity of weak interactions, therefore enhancing the solubility of **ISO** in a hydrophilic environment in the presence of **R2** (Fig. 3). For the same guest, the solubility is markedly enhanced with **R1** than **R2**, which can be explained in terms of better host–guest complementarity of **R1** for host–guest interactions than **R2**. A similar trend in particle size distribution was observed with both hosts, **R1** and **R2** when mixed with **CAF**. The particle sizes of **CAF** in the presence of either host were skewed towards that of the host, thereby imparting the water-soluble effects of the hosts on **CAF** (Fig. S14 and S15†).

Results from NMR measurements indicate that in solution, the complexes are in rapid equilibrium with the free components. Therefore, only one set of signals is observed in the NMR spectra of the mixtures. Despite the dynamic system and fast exchange process, *endo*-cavity binding of the guests can be determined by monitoring the shielding effects of the guest signals. Lower ppm values (shielding) of a guest's proton signals signify a guest predominantly in the cavity of the receptor. In addition, the orientation of the guest within the cavity can be inferred by comparing the degree of shielding of the guest protons with the effect greater for those deeper in the cavity of the receptor. The binding of **CAF** to either **R1** or **R2** led to the shielding of the **CAF** protons, which is indicative of the binding of **CAF** within the cavities of the macrocycles, **R1** and **R2** most likely through hydrophobic effects. At lower equivalents of the guest, more significant shielding of the signals is observed since most of the guests are bound by the host in a fast exchange process. Larger shielding of **CAF** protons was observed with **R2** compared to **R1**. This can be attributed to the size match and aromaticity of **R2**, which complement **CAF** and promote more π–π stacking than **R1**. In contrast, **R1** has fewer flexible groups on its upper rim (Fig. 4 and S7–S10†).

Deshielding of **ISO** guest protons was observed in macrocycle **R2**, indicating binding interactions on the surface of **R2** *via* π–π interactions (Fig. 5). Comparatively, less shielding of **ISO** aromatic protons was observed with **R1**, indicating binding inside the hydrophobic cavity of **R1** *via* π–π stacking. The difference in binding dynamics can be attributed to the flexibility of the upper rim substituents in **R2** compared to **R1**. Poor aqueous solubility of **GRI** at concentrations suitable for NMR did not favor NMR measurements in water. Dissolution in DMSO, however, barred the detection of signal changes due to

Table 3 Statistical analysis for the main compounds assayed in Fig. 6 for inferred cytotoxicity (MTT assay). Compounds are assayed alone or in combination with **R2** at increasing concentrations up to 2000 μM for 24 (left) or 72 (right) hours. Data are representative of at least three biological replicates (mean ± SD), in technical triplicates. Two-way ANOVA Tukey's multiple comparison test

Tukey's multiple comparison test (24 h, **R2**)	Summary	Adjusted *P* value	Tukey's multiple comparison test (72 h, **R2**)	Summary	Adjusted *P* value
6 μM			6 μM		
R2 + **ISO** *vs.* **ISO**	ns	>0.9999	**R2** + **ISO** *vs.* **ISO**	ns	>0.9999
R2 + **CAF** *vs.* **CAF**	**	0.0054	**R2** + **CAF** *vs.* **CAF**	ns	0.9954
R2 + **GRI** *vs.* **GRI**	ns	>0.9999	**R2** + **GRI** *vs.* **GRI**	ns	0.3016
20 μM			20 μM		
R2 + **ISO** *vs.* **ISO**	ns	>0.9999	**R2** + **ISO** *vs.* **ISO**	ns	0.9586
R2 + **CAF** *vs.* **CAF**	**	0.0029	**R2** + **CAF** *vs.* **CAF**	ns	0.9981
R2 + **GRI** *vs.* **GRI**	ns	>0.9999	**R2** + **GRI** *vs.* **GRI**	ns	0.2851
60 μM			60 μM		
R2 + **ISO** *vs.* **ISO**	ns	>0.9999	**R2** + **ISO** *vs.* **ISO**	ns	0.9968
R2 + **CAF** *vs.* **CAF**	****	<0.0001	**R2** + **CAF** *vs.* **CAF**	ns	0.4858
R2 + **GRI** *vs.* **GRI**	**	0.0093	**R2** + **GRI** *vs.* **GRI**	ns	>0.9999
200 μM			200 μM		
R2 + **ISO** *vs.* **ISO**	ns	0.9977	**R2** + **ISO** *vs.* **ISO**	ns	0.9091
R2 + **CAF** *vs.* **CAF**	****	<0.0001	**R2** + **CAF** *vs.* **CAF**	ns	0.9985
R2 + **GRI** *vs.* **GRI**	**	0.0022	**R2** + **GRI** *vs.* **GRI**	ns	0.7590
600 μM			600 μM		
R2 + **ISO** *vs.* **ISO**	ns	0.2616	**R2** + **ISO** *vs.* **ISO**	ns	0.0646
R2 + **CAF** *vs.* **CAF**	ns	0.1685	**R2** + **CAF** *vs.* **CAF**	ns	0.3215
R2 + **GRI** *vs.* **GRI**	****	<0.0001	**R2** + **GRI** *vs.* **GRI**	ns	0.6855
2000 μM			2000 μM		
R2 + **ISO** *vs.* **ISO**	*	0.0464	**R2** + **ISO** *vs.* **ISO**	ns	0.1048
R2 + **CAF** *vs.* **CAF**	****	<0.0001	**R2** + **CAF** *vs.* **CAF**	****	<0.0001
R2 + **GRI** *vs.* **GRI**	ns	0.9818	**R2** + **GRI** *vs.* **GRI**	****	<0.0001

the more hydrophilic nature of DMSO, which prevents possible hydrophobic interactions between **GRI** and either **R1** or **R2**.

Quantification and binding thermodynamics were obtained from a series of ITC experiments. Complex formation between any combination of the hosts' **Rn** and the drug guests is spontaneous ($\Delta G < 0$) at the experimental temperature (298 K) (Table 1 and Fig. S11–S13†). Spontaneous associations between resorcinarenes and guest molecules, such as quinoline, naphthalene, pyrophosphates, *N*-oxides, and heparin in water, have been reported.[36–38,50,51] The positive ΔH and $T\Delta S$ values indicate that the complexation of the guests by **R1** and **R2** is driven mainly by entropy. Desolvation of guest species because of their poor solubility in water may account for the entropy-driven complexations. Only associations between **CAF** and the hosts are both enthalpy and entropy-driven. The highest binding affinity among all the guests was observed with **ISO** on the first binding sites with **R1** ($K_a = 2.11 \times 10^5\ M^{-1}$) (Table 1) which may be due to its ability to fit well into the cavity of the host.

Once it was established that the cell culture was mycoplasma-free, MTT and crystal violet assays were performed to test the compounds' possible cytotoxic effect using the human cell line HEK-293, a well-established model for drug discovery.[52,53]

The MTT assay is usually used to infer cell cytotoxicity and cell proliferation, but also measures cell metabolic activity. More specifically, it measures mainly but not exclusively, the activity of the mitochondrial succinic dehydrogenases.[54,55] Usually, in drug discovery, the hit compounds are tested up to 10 μM concentration.[56,57] However, it is preferable to reach higher concentrations to better understand the effects of the compounds under investigation. This approach guides the researchers in selecting the optimal concentration range for further studies. Data showed that none of the compounds exerted a significant cytotoxic activity at lower concentrations compared to the negative control (Fig. 6). More in detail, isoniazid, the gold standard treatment for tuberculosis, is associated with a well-known hepatotoxicity side effect that may be severe in rare cases, leading to liver failure.[58,59] Cytotoxicity studies in Chinese hamster V97 cell lines showed decreased viability up to about 40% at 50 μM and between 60 and 80% at 200 μM isoniazid concentration at 24 hours.[60] Our data confirmed that the inferred viability is between 60 and 80% at a concentration of 200 μM at 24 hours of treatment, as reported in the literature.[60] Our study showed that isoniazid alone decreases MTT activity, remaining slightly above 50% at a concentration of 2000 μM, both at 24 and 72 hour treatment (Fig. 6A and C). The co-treatment with **R1** or **R2** and isoniazid

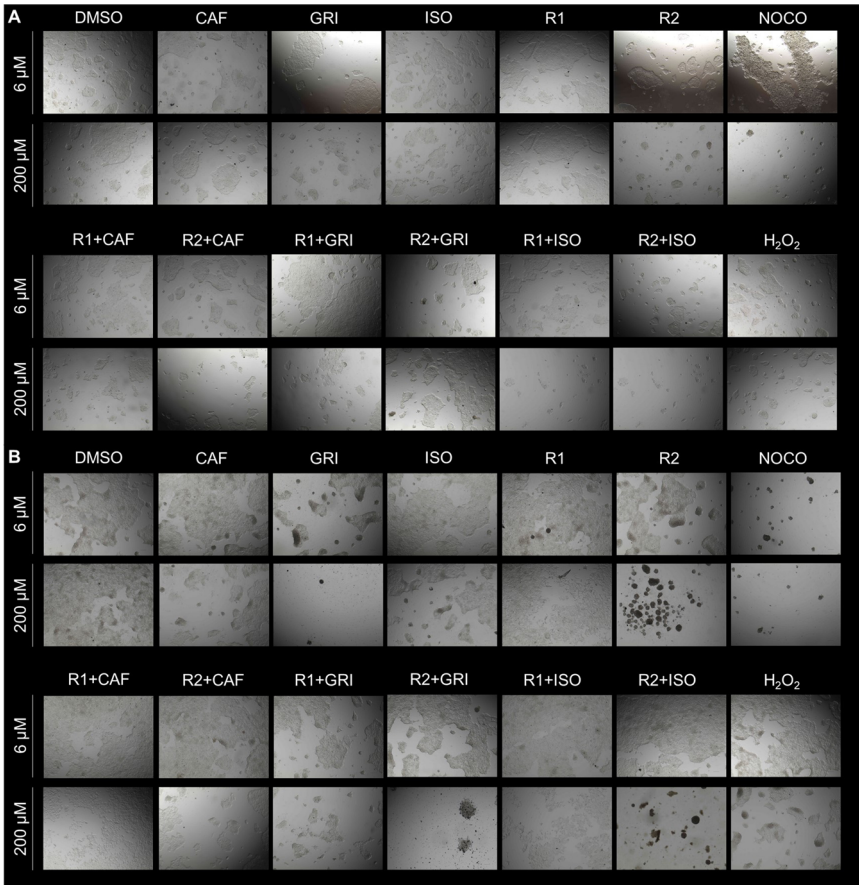

Fig. 7 Compounds assayed for inferred cytotoxicity (qualitative crystal violet assay). HEK-293 cells were incubated with a combination of carriers R1 or R2 and CAF or GRI or ISO to infer cytotoxicity *via* crystal violet assay. Cells are incubated with compounds at 6 or 200 µM for 24 (A) or 72 (B) hours. Nocodazole or H_2O_2 serve as positive control. Data are representative of at least three biological replicates.

together (**R1** + **ISO** or **R2** + **ISO**) decreases the MTT activity at concentrations higher than 600 µM, at 24 (Fig. 6A and B) and 72 hours (Fig. 6C and D).

In literature, it has been shown that caffeine (**CAF**) decreases cell proliferation in mammalian epithelial MCF-7 cell lines, starting at a lower concentration of 80 µM and reaching a low proliferation rate between 37 and 50% at concentrations equal to 5 mM in a bimodal fashion.[61] Our data showed that caffeine alone decreases MTT activity starting at concentrations between 20 and 60 µM but MTT values remain above 50%, both at 24- and 72 hours treatment (Fig. 6A and C). The co-treatment with **R1** or **R2** and caffeine together (**R1** + **CAF** or **R2** + **CAF**) decreases the MTT activity at concentrations higher than 600 µM, at 24 (Fig. 6A and B) and 72 hours (Fig. 6C and D).

Griseofulvin (**GRI**), an antifungal treatment, has been reported for its carcinogenicity in murine models[62,63] and for treatments up to 100 µM for 24 hours.[64,65] Our data confirm **GRI** cytotoxicity at concentrations lower than 100 µM that are attenuated by the co-treatment of **R1** and **R2** for up to 24 hours (Fig. 6A and B). It can be inferred that, **R1** and **R2** alone up to 24 hours significantly decrease the MTT activity in a dose- and time-dependent fashion (Tables 2 and 3). This effect is less evident at an increasing time of up to 72 hours (Tables 2 and 3), likely because of a decreased bioavailability of the compound. Co-treatment with **ISO** and **R1** significantly decreases mitochondrial activity percentage compared to **ISO** alone at higher concentrations (above 600 µM at 24 hours and 200 µM at 72 hours). **ISO**, when complexed with **R2**, affects cells similarly to **ISO** alone, eventually causing a remarkable cytotoxic effect at concentrations exceeding 600 µM (Tables 2 and 3). **CAF**, in combination with **R1** or **R2**, is exerting a significant cytotoxic activity between 600 and 2000 µM (Tables 2 and 3). In comparison, **CAF** alone slightly decreases the MTT activity around 20 to 60 µM to then keep the activity percentages quite constant up to 2000 µM (Tables 2 and 3). Cells treated for 24 hours with **GRI** alone show a decreased inferred viability in a dose- and time-dependent manner, while at 72 hours, the effect reaches a plateau of around 200 µM (Tables 2 and 3). The cytotoxic effect exerted by **GRI** in combination with **R1** or **R2** is markedly increased at prolonged treatment up to 72 hours compared to 24 hours (Tables 2 and 3).

It is usually recommended to use an orthologue approach to confirm the results obtained *via* MTT assay.[66,67] For this purpose, a crystal violet assay has been performed. Cells exposed to cytotoxic compounds lose attachment resulting in a decreased number of cells.[68,69] The inferred cell death is

directly proportional to the decreased optical density (OD) values.[70] Data collected in brightfield qualitatively show the appearance of the cells in the wells before the crystal violet staining (Fig. 7) and support the quantification of the assay (S16).

Data show that all the compounds at both lower (6 μM) and higher (200 μM) concentrations do not show cytotoxicity compared to DMSO (Fig. 7A and S16A†). However, at a longer exposure (72 hours), **GRI** alone or combined with both carriers **R1** or **R2** showed increased cytotoxicity at higher concentrations (200 μM). Carrier **R2** alone or combined with **ISO** at 72 hours of treatment at 200 μM seems to exert a cytotoxic effect on the cells (Fig. 7B). Even though the cells may still be attached to the surface of the plate and retain crystal violet dye (Fig. S16B†), they seem round and clustered (Fig. 7B). This peculiar morphology is usually a clear sign of cell damage.[71]

Conclusions

The complexation of the drug compounds with the ionic resorcinarenes results in shifts of particle sizes of drug compounds towards that of the macrocycles. Such associations produced significant chemical shifts and binding affinities in the micromolar range, which was sufficient to produce a clearer solution of a drug-resorcinarene mixture compared to pure aqueous solutions of drug compounds. Cytotoxicity assessments revealed that resorcinarenes alone or together with drug compounds yielded non-toxic effects, especially at lower and experimental concentrations, confirming the potential of these poly-ionic resorcinarenes to be used as safe and cheaper drug solubilizing agents in the pharmaceutical industry. Cells treated with all the compounds of interest showed signs of decreased metabolism at higher concentrations and extended treatment time. Orthologue approaches regarding the cytotoxicity studies show that cell damage or cell death is increased when cells are treated with a higher concentration (200 μM) of griseofulvin alone or in combination with carrier **R1** or **R2**, and **R2** alone or in combination with isoniazid up to 72 hours treatment. The results show promise in using cavity-containing organic macrocycles as transport and delivery agents for non-water-soluble drugs.

Data availability

The data supporting this article have been included as part of the ESI.†

Author contributions

The manuscript was written and edited with contributions from all authors. All authors have approved the final version of the manuscript. Frank Boateng Osei: original concept, NMR, ITC, and DLS measurements. Wrote sections of the manuscript. Kwaku Twum: original concept, NMR, ITC, and DLS measurements. Wrote sections of the manuscript. Barbara Manfredi: cytotoxicity measurements and wrote the section. Mariana Fatohi: undergrad student, ^{1}H NMR, and ITC measurements. Yvonne Bessem Ojong: supervision, wrote, read, and corrected the manuscript. Valance Washington: supervised the cytotoxicity work. Ngong Kodiah Beyeh: supervised the work.

Conflicts of interest

There are no conflicts to declare.

Acknowledgements

Acknowledgment is made to the donors of the American Chemical Society Petroleum Research Fund (#65027-DNI10) for support (or partial support), the National Science Foundation (#2236984), the National Institute of Health (R01 HL090933), and Oakland University for this research.

Notes and references

1 Y. K. Agrawal and R. N. Patadia, *Rev. Anal. Chem.*, 2006, **25**, 155–239.
2 P. Ziaja, A. Krogul, T. S. Pawłowski and G. Litwinienko, *Thermochim. Acta*, 2016, **623**, 112–119.
3 O. D. Fox, J. Cookson, E. J. S. Wilkinson, M. G. B. Drew, E. J. Maclean, S. J. Teat and P. D. Beer, *J. Am. Chem. Soc.*, 2006, **128**, 6990–7002.
4 K. Twum, K. N. Truong, F. B. Osei, C. von Essen, S. Nadimi, J. F. Trant, K. Rissanen and N. K. Beyeh, *Cryst. Growth Des.*, 2022, **23**, 1281–1287.
5 N. K. Beyeh, D. P. Weimann, L. Kaufmann, C. A. Schalley and K. Rissanen, *Chem.–Eur. J.*, 2012, **18**, 5552–5557.
6 R. Kashapov, Y. Razuvayeva, A. Ziganshina, A. Lyubina, S. Amerhanova, A. Sapunova, A. Voloshina, I. Nizameev, V. Salnikov and L. Zakharova, *Colliods Surf., A*, 2022, **648**, 129330–129338.
7 A. Halder, D. C. Mukherjee and S. Bhattacharya, *J. Solution Chem.*, 2010, **39**, 1327–1340.
8 W. C. Geng, J. L. Sessler and D. S. Guo, *Chem. Soc. Rev.*, 2020, **49**, 2303–2315.
9 F. Jia, H. V Schrö, L. P. Yang, C. Von Essen, S. Sobottka, B. Sarkar, K. Rissanen, W. Jiang and C. A. Schalley, *J. Am. Chem. Soc.*, 2020, **142**, 3306–3310.
10 S. Ohtani, K. Kato, S. Fa and T. Ogoshi, *Coord. Chem. Rev.*, 2022, **462**, 214503–214511.
11 G. Wenz, *Clin. Drug Invest.*, 2000, **19**, 21–25.
12 O. Kretschmann, C. Steffens and H. Ritter, *Angew. Chem., Int. Ed.*, 2007, **46**, 2708–2711.
13 H. Wen, H. Jung and X. Li, *AAPS J.*, 2015, **17**, 1327–1340.
14 C. M. O'Driscoll and B. T. Griffin, *Adv. Drug Deliv. Rev.*, 2008, **60**, 617–624.
15 R. Samineni, J. Chimakurthy and S. Konidala, *Turk. J. Pharm. Sci.*, 2022, **19**, 706–713.
16 F. Wu, R. Cristofoletti, L. Zhao and A. Rostami-Hodjegan, *Biopharm. Drug Dispos.*, 2021, **42**, 118–127.
17 D. C. Vimalson, S. Parimalakrishnan, N. S. Jeganathan and S. Anbazhagan, *Asian J. Pharm.*, 2016, **10**, 67–76.
18 D. V. Bhalani, B. Nutan, A. Kumar and A. K. S. Chandel, *Biomedicines*, 2022, **10**, 2055–2087.

19 S. M. Abuzar, S. M. Hyun, J. H. Kim, H. J. Park, M. S. Kim, J. S. Park and S. J. Hwang, *Int. J. Pharm.*, 2018, **538**, 1–13.
20 J. S. Kim, H. Park, K. T. Kang, E. S. Ha, M. S. Kim and S. J. Hwang, *J. Pharm. Invest.*, 2022, **52**, 353–366.
21 R. Jayalakshmy, K. S. Sreethu and C. R. Jayalakshmy, *J. Med. Pharm. Allied Sci.*, 2021, **3**, 2763–2771.
22 J. B. Ngilirabanga and H. Samsodien, *Nano Select*, 2021, **2**, 512–526.
23 S. Sareen, L. Joseph and G. Mathew, *Int. J. Pharm. Invest.*, 2012, **2**, 12–17.
24 M. N. S. Patel, M. H. Ahmed, M. Saqib and S. N. Shaikh, *J. Drug Delivery Ther.*, 2019, **9**, 542–546.
25 A. K. Gupta and C. Drummond-Main, *Pediatr. Dermatol.*, 2013, **30**, 1–6.
26 Y. Fujioka, Y. Metsugi, K. I. Ogawara, K. Higaki and T. Kimura, *Int. J. Pharm.*, 2008, **352**, 36–43.
27 V. Pittol, K. S. Veras, S. Kaiser, L. J. Danielli, A. M. Fuentefria and G. G. Ortega, *Braz. J. Pharm. Sci.*, 2022, **58**, 1–13.
28 R. Kumar, *J. Drug. Deliv. Sci. Technol.*, 2019, **53**, 101221–101228.
29 D. Yang, R. Kulkarni, R. J. Behme and P. N. Kotiyan, *Int. J. Pharm.*, 2007, **329**, 72–80.
30 C. Becker, J. B. Dressman, G. L. Amidon, H. E. Junginger, S. Kopp, K. K. Midha, V. P. Shah, S. Stavchansky and D. M. Barends, *J. Pharm. Sci.*, 2007, **96**, 522–531.
31 B. Xuan, S. N. Wong, Y. Zhang, J. Weng, H. H. Y. Tong, C. Wang, C. C. Sun and S. F. Chow, *Cryst. Growth Des.*, 2020, **20**, 1951–1960.
32 V. Reddy and M. Saharay, *J. Phys. Chem. B*, 2019, **123**, 9685–9691.
33 I. Shumilin, C. Allolio and D. Harries, *J. Am. Chem. Soc.*, 2019, **141**, 18056–18063.
34 L. Lomba, A. Polo, J. Alejandre, N. Martínez and B. Giner, *J. Drug Delivery Sci. Technol.*, 2023, **79**, 104010–104017.
35 D. M. Galindres, D. Cifuentes, L. E. Tinoco, Y. Murillo-Acevedo, M. M. Rodrigo, A. C. F. Ribeiro and M. A. Esteso, *Processes*, 2022, **10**, 684–697.
36 A. Karle, K. Twum, N. Sabbagh, A. Haddad, S. M. Taimoory, M. M. Szczęśniak, E. Trivedi, J. F. Trant and N. K. Beyeh, *Analyst*, 2022, **147**, 2264–2271.
37 K. Twum, N. Schileru, B. Elias, J. Feder, L. Yaqoo, R. Puttreddy, M. M. Szczesniak and N. K. Beyeh, *Symmetry*, 2020, **12**, 1–8.
38 K. Twum, S. I. Sadraei, J. Feder, S. M. Taimoory, K. Rissanen, J. F. Trant and N. K. Beyeh, *Org. Chem. Front.*, 2022, **9**, 1267–1275.
39 P. Singla, O. Singh, S. Sharma, K. Betlem, V. K. Aswal, M. Peeters and R. K. Mahajan, *ACS Omega*, 2019, **4**, 11251–11262.
40 P. C. Griffiths, B. Cattoz, M. S. Ibrahim and J. C. Anuonye, *Eur. J. Pharm. Biopharm.*, 2015, **97**, 218–222.
41 E. Vaculikova, A. Cernikova, D. Placha, M. Pisarcik, P. Peikertova, K. Dedkova, F. Devinsky and J. Jampilek, *Molecules*, 2016, **21**, 1005–1012.
42 Á. Sarabia-Vallejo, M. M. Caja, A. I. Olives, M. A. Martín and J. C. Menéndez, *Pharmaceutics*, 2023, **15**, 2345–2397.
43 K. Ueda, K. Higashi, W. Limwikrant, S. Sekine, T. Horie, K. Yamamoto and K. Moribe, *Mol. Pharm.*, 2012, **9**, 3023–3033.
44 I. Ghiviriga, *Anal. Chem.*, 2023, **95**, 2706–2712.
45 K. Ueda and L. S. Taylor, *Mol. Pharm.*, 2020, **17**, 1352–1362.
46 R. Patel, G. Buckton and S. Gaisford, *Thermochim. Acta*, 2007, **456**, 106–113.
47 A. I. Rodriguez-Perez, C. Rodriguez-Tenreiro, C. Alvarez-Lorenzo, P. Taboada, A. Concheiro and J. J. Torres-Labandeira, *J. Pharm. Sci.*, 2006, **95**, 1751–1762.
48 K. Twum, A. Bhattacharjee, E. T. Laryea, J. Esposto, G. Omolloh, S. Mortensen, M. Jaradi, N. L. Stock, N. Schileru, B. Elias, E. Pszenica, T. M. McCormick, S. Martic and N. K. Beyeh, *RSC Med. Chem.*, 2021, **12**, 2022–2030.
49 M. R. Patel, D. A. Lamprou and P. R. Vavia, *AAPS PharmSciTech*, 2020, **11**, 1–16.
50 K. Twum, S. Nadimi, F. B. Osei, R. Puttreddy, Y. B. Ojong, J. J. Hayward, K. Rissanen, J. F. Trant and N. K. Beyeh, *Chem. Asian J.*, 2023, **18**, 1308–1320.
51 S. Välimäki, N. K. Beyeh, V. Linko, R. H. A. Ras and M. A. Kostiainen, *Nanoscale*, 2018, **10**, 14022–14030.
52 A. Heding, *Expert Rev. Mol. Diagn.*, 2004, **4**, 403–411.
53 L. Ho, C. L. Greene, A. W. Schmidt and L. H. Huang, *Cytotechnology*, 2004, **45**, 117–123.
54 P. L. Tseng, W. H. Wu, T. H. Hu, C. W. Chen, H. C. Cheng, C. F. Li, W. H. Tsai, H. J. Tsai, M. C. Hsieh, J. H. Chuang and W. T. Chang, *Sci. Rep.*, 2018, **8**, 3081–3096.
55 A. Kumar, Y. Rai and A. N. Bhatt, *Cytotechnology*, 2024, **76**, 301–311.
56 K. Katsuno, J. N. Burrows, K. Duncan, R. H. V. Huijsduijnen, T. Kaneko, K. Kita, C. E. Mowbray, D. Schmatz, P. Warner and B. T. Slingsby, *Nat. Rev. Drug Discovery*, 2015, **14**, 751–758.
57 S. Bendels, C. Bissantz, B. Fasching, G. Gerebtzoff, W. Guba, M. Kansy, J. Migeon, S. Mohr, J. U. Peters, F. Tillier, R. Wyler, C. Lerner, C. Kramer, H. Richter and S. Roberts, *J. Pharmacol. Toxicol. Methods*, 2019, **99**, 106609–106616.
58 W. K. Kabbara, A. T. Sarkis and P. G. Saroufim, *Case Rep. Infect. Dis.*, 2016, **2016**, 3617408–3617413.
59 I. Metushi, J. Uetrecht and E. Phillips, *Br. J. Clin. Pharmacol.*, 2016, **81**, 1030–1036.
60 D. Kakkar, A. K. Tiwari, K. Chuttani, A. Khanna, A. Datta, H. Singh and A. K. Mishra, *Chem. Biol. Drug Des.*, 2012, **80**, 245–253.
61 A. Kazaks, M. Collier and M. Conley, *Curr. Dev. Nutr.*, 2019, **3**, 31–38.
62 P. Aris, Y. Wei, M. Mohamadzadeh and X. Xia, *Molecules*, 2022, **27**, 7034–7041.
63 M. Rustia and P. Shubik, *Br. J. Cancer*, 1978, **38**, 237–249.
64 S. Gupta, A. Kumar and K. K. Tejavath, *Mol. Biol. Rep.*, 2021, **48**, 2945–2956.
65 A. B. Petersen, G. Konotop, N. H. M. Hanafiah, P. Hammershøj, M. S. Raab, A. Krämer and M. H. Clausen, *Eur. J. Med. Chem.*, 2016, **116**, 210–215.
66 Y. Li, S. Lam, J. C. Mak, C. Zheng and J. C. M. Ho, *Lung Cancer*, 2013, **81**, 354–361.

67 W. Hu, Q. Liu, J. Pan and Z. Sui, *Biomed. Pharmacother.*, 2018, **105**, 887–898.
68 F. Wei, S. Wang and X. Gou, *Biophys. Rep.*, 2021, **7**, 504–516.
69 M. Feoktistova, P. Geserick and M. Leverkus, *Cold Spring Harb. Protoc.*, 2016, **2016**, 343–346.
70 T. V. Berghe, S. Grootjans, V. Goossens, Y. Dondelinger, D. V. Krysko, N. Takahashi and P. Vandenabeele, *Methods*, 2013, **61**, 117–129.
71 S. Elmore, *Toxicol. Pathol.*, 2007, **35**, 495–516.